

Ionization Induced Trapping in a Laser Wakefield Accelerator

C. McGuffey, A. G. R. Thomas, W. Schumaker, T. Matsuoka, V. Chvykov, F. J. Dollar, G. Kalintchenko, V. Yanovsky, A. Maksimchuk, and K. Krushelnick

Center for Ultrafast Optical Science, The University of Michigan, Ann Arbor, Michigan 48109, USA

V. Yu. Bychenkov

P. N. Lebedev Physics Institute, Russian Academy of Science, Leninskii Prospect 53, Moscow 119991, Russia

I. V. Glazyrin and A. V. Karpeev

RFNC-VNIITF, Snezhinsk 456770, Chelyabinsk region, Russia

(Received 3 August 2009; published 15 January 2010)

Experimental studies of electrons produced in a laser wakefield accelerator indicate trapping initiated by ionization of target gas atoms. Targets composed of helium and controlled amounts of various gases were found to increase the beam charge by as much as an order of magnitude compared to pure helium at the same electron density and decrease the beam divergence from 5.1 ± 1.0 to 2.9 ± 0.8 mrad. The measurements are supported by particle-in-cell modeling including ionization. This mechanism should allow generation of electron beams with lower emittance and higher charge than in preionized gas.

DOI: 10.1103/PhysRevLett.104.025004

PACS numbers: 52.38.Kd, 52.25.Jm

In a laser wakefield accelerator [1], an intense ultrashort laser pulse generates a plasma wave, known as a wakefield, with a phase velocity close to the speed of light. A relativistic electron beam copropagating with the wakefield can therefore remain in an accelerating phase of the wave for a relatively long distance, and extract a large energy gain from its longitudinal electric field. Plasma waves can support electric fields many orders of magnitude stronger than those in radio-frequency cavities, and hence should provide a compact alternative, or complement, to conventional electron accelerators in the future.

In the strongly nonlinear regime, the laser pulse expels electrons from its focal volume [2] but has a negligible effect on the ions, which remain, resulting in a cavity with strong electromagnetic fields. Electrons from the periphery of the cavity are pulled inwards by the strong Coulomb attraction and form a thin high-density sheath around an approximately spherical “bubble” [3,4]. This bubble has ideal accelerating and focusing properties for electrons within the cavity [5], and at the point where the sheaths cross at the rear of the bubble, the field is particularly strong. Here, electrons can be accelerated to the phase velocity of the bubble in a time shorter than their crossing time and are therefore trapped. Under certain conditions, the trapped electron beam can have a quasimonoenergetic energy distribution [6–9].

Control of the onset of this self-trapping is not independent of the accelerated electron beam charge, peak energy and emittance, as all of these depend on the drive laser pulse characteristics and global plasma density [10]. Initiating trapping independently of the acceleration process can be performed by implementing an external injection source of electrons [11] or using an additional laser pulse to cause injection [12–15]. In reference [12], the

proposed mechanism was to use a second high intensity laser to field ionize electrons within the wake to initiate trapping. A related ionization trapping mechanism has been demonstrated in electron beam driven plasma wave accelerator experiments on the Stanford Linear Collider (SLAC) [16]. Ionization induced trapping was inferred in experiments on laser wakefield acceleration in a capillary due to migration of high Z wall ions to the laser axis [17].

The self-trapping condition is that an electron gains sufficient forward momentum from the longitudinal electric field to reach the phase velocity of the bubble before it slips out of the accelerating phase. Creation of free electrons by ionization, initially at rest within the electron cavity, can initiate trapping because these electrons experience additional energy gain due to the net potential difference between the edge of the bubble and its interior. This translates to a lowered trapping threshold, and is maximized if the electrons are initiated at the minimum of the potential.

Presented here is the first experimental demonstration of electron trapping initiated by ionization in a laser wakefield accelerator. We show that this mechanism increases the trapped charge by up to an order of magnitude and decreases the emittance of the electron beam generated. A range of noble gases, and nitrogen, is systematically added as a small percentage to helium gas. It is determined that optical field ionization of inner shell electrons of the higher Z gas plays an important role in moderating the trapped charge. Although there is a small increase in electron number density due to the higher Z gas additive, it is shown to be insufficient to account for the increase in charge in the trapped bunch. In addition, the behavior of the trapping is consistent with the field-ionization thresholds for the various gas species added to the helium. Improvements in

beam charge and emittance are important for applications such as x-ray generation through inverse Compton scattering, or free electron lasers, as well as x-ray generation by oscillation in a plasma based wiggler. By using a gas mixture, lower power laser systems can be used to generate higher charge, higher energy, and decreased emittance monoenergetic electron beams than can be produced using a fully preionized plasma.

In these experiments, pulses from the HERCULES laser system [18] at the University of Michigan (30 fs, 800 nm Ti:sapphire) were focused using an $f/10$ off-axis parabolic mirror onto the edge of gas flow from a 3 mm diameter conical supersonic nozzle. The laser wave front was corrected with a deformable mirror, yielding a focused spot of 10 μm full-width-half-maximum (FWHM). The experiments were conducted using a laser peak power ranging from 24–120 TW on target. The focused peak intensity was $I = 3.5 \times 10^{19}$ at 30 TW and $I = 1.5 \times 10^{20}$ at 120 TW. Diagnostics included an electron beam profile monitor and an electron spectrometer (0.8 T removable magnet, two Lanex phosphor screens) with electron energy detection range of 47–800 MeV. A transverse probe beam was used for transverse interferometry. Sidescattered light from the plasma was split with a wedge and sent to an imaging CCD as well as a spectrometer with 260 nm spectral window centered around the laser wavelength. Gas was pulsed from a solenoid valve (5 ms opening time) through the gas nozzle. Gases added to the helium target included air, nitrogen, neon, argon, krypton, and xenon.

To ensure a homogeneous mixture, the gases were agitated in a 2.5 l steel vessel. The vessel and all gas lines were evacuated before introducing any gases. Care was taken to eliminate leaks in the lines. In order to accurately produce low additive to helium ratio mixtures, the gas additive was introduced using a low pressure regulator (typically <4 atm) first, and subsequently helium was added at high pressure (67 atm) from an isolated supply. A third regulator was installed on the output of the mixing vessel, maintaining constant pressure for many tens of shots with the same gas mixture. Before a typical experimental run, air contaminant can be introduced into the gas as a result of changing regulators or gas bottles. However for these experiments many gases were installed on a manifold so that air would not be introduced when changing gases. A density scan was conducted with each gas mixture ratio for a number of different ratios of additive to helium, between 0:1 and 5:95 by partial pressure. Electron number density was monitored via both transverse interferometry and Raman-shifted scattered light. Electron plasma densities in the range 5×10^{18} – $3 \times 10^{19} \text{ cm}^{-3}$ were investigated.

Certain gas mixtures significantly improved the probability of injecting electrons and also increased the amount of charge in the electron beam relative to pure helium. However, it is important to accurately diagnose the exact electron number density in the interaction with the higher Z additive. Strong sidescatter was emitted throughout the front (approximately one Rayleigh range) of the plasma.

The wavelength of the scattered light was observed to be shifted to the red of the initial laser wavelength, λ_0 , according to $(\Delta\lambda/\lambda_s)^2 \propto n_e$, where n_e is electron number density, λ_s is the redshifted wavelength and $\Delta\lambda$ is $\lambda_s - \lambda_0$. The gas mixture ratios are defined by the absolute pressure of the gas additive relative to the absolute pressure of helium. For each 1% increase in additive mixture of a gas with n electrons which can be ionized the electron density will increase by $(n - 2)\%$ relative to helium gas at the same pressure. Electron densities quoted in this Letter are calculated according to the above discussion, as some interferometry images were blinded by sidescattered light particularly when laser power was >100 TW. In these instances Raman-shifted scattered light provided a secondary measurement of electron density. Both measurements were shown to agree with the calculated electron density within the uncertainties of the gas pressures.

The effect of gas additives on beam charge is shown in Fig. 1. In shots using 30 TW laser power, a nitrogen additive consistently led to an increase in the total integrated charge of almost an order of magnitude compared to a pure He target with equal electron density, Fig. 1(a). For example, the first data point on the series labeled He + N₂ in Fig. 1(a) includes data from shots at 30 TW containing 1.2% N₂ and 98.8% He by pressure at a total pressure of 150 psig. Pure He at 175 psig yields the same electron density but no detectable beams. Using a slightly lower

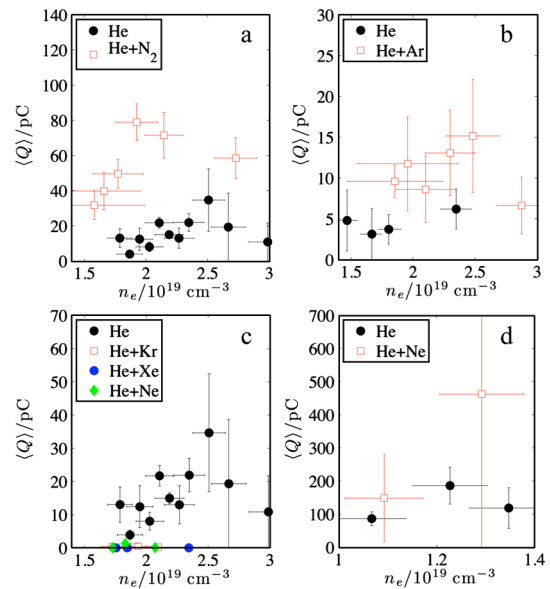


FIG. 1 (color online). Integrated charge above 30 MeV measured by the electron spectrometer as a function of electron number density. The values represent an average of 5–20 shots for which the electron signal is clearly above background. For gas mixtures the electron density increase is due to a change in the proportion of additive to helium while the total gas jet backing pressure is held fixed; for pure helium the electron density increase is due to an increase in backing pressure of pure helium gas. The experiments were performed with a laser power of (a) 30 TW, (b) 24 TW, (c) 30 TW, and (d) 120 TW.

power of 24 TW, argon also showed a substantial charge increase, Fig. 1(b). Neon and other higher Z gas additives consistently decreased the beam charge in all cases at 30 TW, Fig. 1(c). At 120 TW, using neon, an improvement in the mean trapped charge compared with helium was recorded, Fig. 1(d). More interestingly, this behavior was significantly different from the 30 TW case, Fig. 1(c).

These results can be understood by consideration of the optical field ionization thresholds for the different species [19]. Both nitrogen and argon have a number of L -shell or M -shell electrons with a field ionization intensity threshold of $I_{BS} < 10^{17} \text{ W cm}^{-2}$, and can be considered preionized before the formation of the bubble.

However, the K -shell electrons for nitrogen have a threshold intensity for ionization of $I_{BS} \approx 10^{19} \text{ W cm}^{-2}$, and so the majority of these electrons will be freed near the peak of the pulse. Likewise, the L shell of argon has eight electrons with ionization threshold intensities ranging from $10^{18} \lesssim I_{BS} \lesssim 10^{19} \text{ W cm}^{-2}$, and so a proportion of the electrons are expected to be freed near the peak of the pulse. Xenon and krypton have large numbers of outer shell electrons at low ionization thresholds that presumably cause ionization defocusing of the pulse and prevent stable wakefield formation, which could be observed in interferometry images. Neon has an L shell which is fully ionized below an ionization threshold of $I_{BS} < 10^{17} \text{ W cm}^{-2}$, but its K shell is ionized at close to $I_{BS} \approx 10^{20} \text{ W cm}^{-2}$, which is significantly higher than the peak intensity of the laser at 30 TW. This explains the different behavior of neon additive at 120 TW vs 30 TW. For the case $a > 1$, where a is the normalized vector potential, the peak bubble electric field scales like $(\lambda_0/\lambda_p) * E_L$, where λ_p is the plasma wavelength and E_L is the peak laser field, and so is likely 20 or 30 times less than E_L in our experiments. The intensity and species dependent increase in charge is a strong indication of an ionization trapping mechanism with ionization by the laser field.

Adding too much higher Z gas, of any species, was also found to be detrimental to electron injection, also due to ionization defocusing (for example, Fig. 1(b), far right). The mixing chamber apparatus allowed for systematic control necessary for this study. However, by merely exposing the gas lines to a small quantity of air before filling with helium, results similar to the nitrogen additive run were achieved.

Typical electron spectra obtained on the experiment are shown in Fig. 2. Panel (a) shows typical He and He + N₂ spectra superimposed, to demonstrate that the increase in charge is not at the expense of mean energy, for otherwise identical conditions. Figures 2(b) and 2(c) show electron spectra obtained with argon and neon additive, respectively, which are clearly quasimonoenergetic. The mean energy of the electron beams produced by ionization trapping was measured to be the same, within statistical error, as from those produced by self-trapping in helium only. This is to be expected, as ionization should not signifi-

cantly modify the bubble structure due to the bulk of electrons being preionized in all cases studied.

The beam divergence was measured by imaging a Lanex screen placed 1 m behind the target with the magnet removed. Typical profiles are shown in Fig. 3. The mean divergence in the vertical direction was $5.1 \pm 1.0 \text{ mrad}$, averaged over 5 shots for the case of pure helium and $2.9 \pm 0.8 \text{ mrad}$ averaged over 8 shots for He + 1% Ar. The integrated charge from the shots with Ar additive was, on average, twice that of shots with pure He. Although not a measure of the transverse emittance of the beam, it can be inferred that the increased collimation of the beam corresponds to an improved emittance, if a comparable source size is assumed.

To analyze the effect of the ionization dynamics on trapping mechanisms and acceleration of trapped electrons, the two dimensional particle-in-cell code PICNIC was used. In the code, field ionization is accounted for using the Ammosov-Delone-Krainov model [20]. The energy loss to ionization of atoms from the fields is accounted for in Maxwell's equations through an energy balance expression. All electrons are tagged based on the ionization state from which they originate. In a typical run, the spatial grid has 16 cells per laser wavelength, and 20–30 macroparticles per cell.

Numerical calculations were performed for conditions similar to those of the 30 TW experiment, in a gas density of 10^{19} cm^{-3} . Computational runs were performed for (i) a fully ionized helium plasma, (ii) helium gas including field ionization, and (iii) a mixture of 95% helium and 5% nitrogen, including field ionization. As expected, there are no significant differences between cases (i) and (ii). For case (iii) it was found that the spectrum includes a

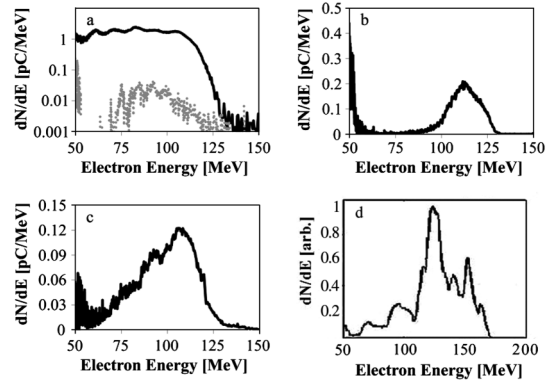


FIG. 2. (a) Electron spectrum from a 30 TW shot with a target of pure helium (grey) is enhanced greatly by a mere 1% N₂ additive (solid black), while the charge-weighted average energy remains the same. Note in this particular graph the scale is logarithmic. The beam can be reasonably monoenergetic at an appropriate density for both the pure He and N₂ cases. (b) Monoenergetic spectrum from a 24 TW shot with 1% Ar additive. (c) Spectrum from a 120 TW shot with 1% Ne additive. (d) Spectrum from particle-in-cell simulation of 30 TW shot with a target of He + 5% N₂.

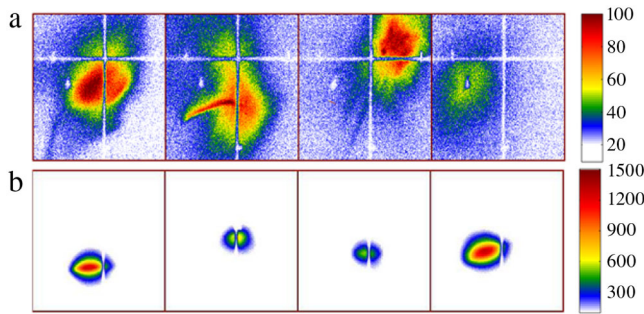


FIG. 3 (color online). Electron beam profiles measured on a Lanex screen 1 m from the target. The top four images, (a), are from shots with pure helium and the bottom four, (b), are from shots with a 1% argon additive, both at equal electron number density $n_e = 2 \times 10^{19} \text{ cm}^{-3}$. Note the difference in color scale, which represents electron signal [arb] per pixel.

high-energy electron bunch which has a peak around 120 MeV after 500 μm propagation, Fig. 2(d). This bunch originates from field ionization of N^{5+} and N^{6+} ions. Figure 4 shows the spatial distribution of electrons near the bubble at $t = 1.0$ ps. In this simulation, these electrons appear through ionization of N^{5+} and N^{6+} , which are ionized primarily in the proximity of the peak of the laser pulse. However, of the electrons from these ionization states, the ones which eventually become trapped all originate slightly off-axis. They then flow into the acceleration region off-axis, as shown by arrows in Fig. 4. Acceleration terminates at 1.5 ps. The total electron beam charge in the case of pure He is 0.57 nC, and 0.83 nC in the case of He + N_2 , in which the electron charge due to He is 0.47 nC. From the He plasma the number of high-energy electrons (with energy >100 MeV) was 2 orders of magnitude less than from He + N_2 plasma.

At 1.0 ps, the bubble is elongated, as seen in Fig. 4. Electrons from helium move along the bubble periphery and reach the region of accelerating field located near axis, at a distance of (50–55) λ_0 from the laser pulse, with typical trajectories shown by arrows (i) in Fig. 4. Electrons produced via field ionization of nitrogen from neutral gas up to N^{4+} move in a similar manner as these states are ionized early in the pulse. However, electrons from ionization of N^{5+} and N^{6+} behave differently, with typical trajectory indicated by arrow (ii) in Fig. 4. They are born in the region of strong focusing magnetic field and result in a jet with large current density (more than 10 times the current density of electrons from helium). It was also found in the simulation that the addition of nitrogen improved the collimation of the electron beam by approximately a factor of 2 which agrees with the experimental results.

In conclusion, ionization induced trapping in a laser driven wakefield accelerator has been systematically investigated by exploring the parameter space of atomic number and impurity concentration. The addition of a higher Z additive has been shown to increase the trapped charge and lower the transverse emittance of the generated

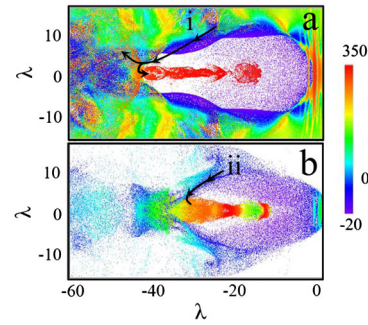


FIG. 4 (color online). Electrons from ionization of (a) He and N through N^{4+} , (b) N^{5+} and N^{6+} . Color represents the longitudinal normalized momentum of the electrons. The spatial coordinates are in units of λ_0 . The arrows schematically exhibit electron trajectories taken from the time series data.

electron beam as compared to pure helium at the same electron density. This should be a useful trapping mechanism for efficiently producing electron beams where stringent constraints on the beam emittance and charge are required such as x-ray production in a plasma or conventional wiggler, as well as to control injection.

This work was supported by the NSF through the Physics Frontier Center FOCUS (Grant No. PHY-0114336) and by the NSF/DNDO (Grant No. F021166).

-
- [1] T. Tajima and J.M. Dawson, Phys. Rev. Lett. **43**, 267 (1979).
 - [2] G.Z. Sun, E. Ott, Y.C. Lee, and P. Guzdar, Phys. Fluids **30**, 526 (1987).
 - [3] A. Pukhov and J. Meyer-ter Vehn, Appl. Phys. B **74**, 355 (2002).
 - [4] W. Lu *et al.*, Phys. Plasmas **13**, 056709 (2006).
 - [5] J. B. Rosenzweig, B. Breizman, T. Katsouleas, and J. J. Su, Phys. Rev. A **44**, R6189 (1991).
 - [6] S. P. D. Mangles *et al.*, Nature (London) **431**, 535 (2004).
 - [7] C. G. R. Geddes *et al.*, Nature (London) **431**, 538 (2004).
 - [8] J. Faure *et al.*, Nature (London) **431**, 541 (2004).
 - [9] E. Miura *et al.*, Appl. Phys. Lett. **86**, 251501 (2005).
 - [10] A. Maksimchuk *et al.*, Appl. Phys. B **89**, 201 (2007).
 - [11] D. Kaganovich *et al.*, Phys. Plasmas **12**, 100702 (2005).
 - [12] D. Umstadter, J. K. Kim, and E. Dodd, Phys. Rev. Lett. **76**, 2073 (1996).
 - [13] E. Esarey, R. F. Hubbard, W. P. Leemans, A. Ting, and P. Sprangle, Phys. Rev. Lett. **79**, 2682 (1997).
 - [14] J. Faure *et al.*, Nature (London) **444**, 737 (2006).
 - [15] A. G. R. Thomas *et al.*, Phys. Rev. Lett. **100**, 255002 (2008).
 - [16] E. Oz *et al.*, Phys. Rev. Lett. **98**, 084801 (2007).
 - [17] T. P. Rowlands-Rees *et al.*, Phys. Rev. Lett. **100**, 105005 (2008).
 - [18] V. Yanovsky *et al.*, Opt. Express **16**, 2109 (2008).
 - [19] S. Augst, D. Strickland, D. D. Meyerhofer, S. L. Chin, and J. H. Eberly, Phys. Rev. Lett. **63**, 2212 (1989).
 - [20] M. V. Ammosov, N. B. Delone, and V. P. Krainov, Zh. Eksp. Teor. Fiz. **91**, 2008 (1986).